2D Materials

PAPER

Ultraflexible and robust graphene supercapacitors printed on textiles for wearable electronics applications

Amr M Abdelkader[1,2], Nazmul Karim[1,3], Cristina Vallés[4], Shaila Afroj[3], Kostya S Novoselov[1,2] and Stephen G Yeates[3]

[1] National Graphene Institute (NGI), University of Manchester, Booth Street East, M13 9PL, Manchester, United Kingdom
[2] School of Physics and Astronomy, University of Manchester, Oxford Road, M13 9PL, Manchester, United Kingdom
[3] School of Chemistry, University of Manchester, Oxford Road, M13 9PL, Manchester, United Kingdom
[4] School of Materials, University of Manchester, Oxford Road, M13 9PL, Manchester, United Kingdom

E-mail: amr.abdelkader@manchester.ac.uk **and** aa494@cam.ac.uk

Keywords: graphene, smart textiles, supercapacitors, wearable devices, screen printing

Supplementary material for this article is available online

OPEN ACCESS

RECEIVED
31 March 2017

REVISED
26 June 2017

ACCEPTED FOR PUBLICATION
4 July 2017

PUBLISHED
24 July 2017

OPEN ACCESS
8 November 2017

Abstract

Printed graphene supercapacitors have the potential to empower tomorrow's wearable electronics. We report a solid-state flexible supercapacitor device printed on textiles using graphene oxide ink and a screen-printing technique. After printing, graphene oxide was reduced *in situ* via a rapid electrochemical method avoiding the use of any reducing reagents that may damage the textile substrates. The printed electrodes exhibited excellent mechanical stability due to the strong interaction between the ink and textile substrate. The unique hierarchical porous structure of the electrodes facilitated ionic diffusion and maximised the surface area available for the electrolyte/active material interface. The obtained device showed outstanding cyclic stability over 10 000 cycles and maintained excellent mechanical flexibility, which is necessary for wearable applications. The simple printing technique is readily scalable and avoids the problems associated with fabricating supercapacitor devices made of conductive yarn, as previously reported in the literature.

Introduction

The rapid development in wearable technology requires a new generation of energy storage devices that satisfy the future design requirements. Examples include military, high-performance sportswear, wearable displays, sensors and other embedded health monitoring devices, new classes of mobile communication devices, and possibly even new classes of wearable computers [1, 2]. To empower these new wearable devices, the energy storage system must have reasonable mechanical flexibility in addition to high energy and power density, good operational safety, long cycling life and be low cost [3, 4]. Among the many energy storage devices available, flexible supercapacitors (SCs) are promising candidates because of their quick charge–discharge capabilities, long life cycles and good safety [5, 6]. This is because SCs directly drives electrical charge in and out of electrical double layers, instead of storing the energy through chemical redox reactions, which is the case for batteries. However, there are many challenges associated with the development of flexible SCs. Some of the issues are related to the active materials, but others are related to the flexible substrate or the device fabrication method [7].

Carbon nanomaterials are commonly used as active materials for flexible SCs [8–11]. Many nanostructured carbon materials, such as 0D carbon nanoparticles [12] and one-dimensional (1D) carbon nanotubes or nanofibers, have been fabricated into electrodes [13]. Carbon nanomaterials are light, mechanically strong and flexible, chemically inert and can be processed to fit micro and nano structural designs [11]. Additionally, carbon-based electrodes are highly conductive, so there is no need to add extra current collectors, conductive additives or binders [11, 14]. With the rise of the graphene era, significant attention has been paid to developing graphene-based flexible SC [15, 16]. Only one atomic layer thick, graphene provides the highest possible specific surface area of all carbon materials (2600 $m^2\ g^{-1}$), delivering a theoretical capacitance as high as 550 $F\ g^{-1}$ [17]. The majority of reported graphene-based SCs use graphene oxide (GO) as a precursor for the affordable and large-scale production of graphene [18–22].

GO-derived materials include functionalised GO [23], reduced GO (rGO) and GO composites [24, 25], and they can be made conductive via several chemical [26], electrochemical [27] and thermal reduction techniques.

Substrate materials play an essential role in the performance of a flexible SC electrode. These substrates are usually selected to provide additional functionality to the device, such as improving the mechanical stability or flexibility, working as a template to provide reasonable electrode porosity and/or working as a current collector. Examples of the various materials that have been used as substrates include nickel foam [28], aluminium foam or foil, graphite sheets, carbon cloths, carbon nanofibers, PET, paper and textile [29]. Amongst them, textile is an ideal substrate for wearable applications due to its high flexibility, good mechanical strength, biocompatibility and low cost. Textiles are porous and flexible material made by weaving or pressing natural or synthetic fibres, such as cotton or polyester. Here we focus our attention on cotton-based textiles since their hierarchical structure and plurality of hydroxyl groups have significant advantages in terms of electrode porosity and adhesion.

Another challenge in the development of graphene-based flexible SCs is the electrode manufacturing procedures. During fabrication, the graphene flakes tend to agglomerate together by van der Waal forces and form dense clusters, resulting in a reduction of the accessible surface area [30]. Even in the best cases, the obtained gravimetric specific capacitance is only slightly less than half of the theoretical value. Many methods have been reported in the literature to prepare flexible graphene electrodes, including electrodeposition, direct coating by drop casting or spray coating, chemical vapour deposition, vacuum filtration, *in situ* polymerisation and self-assembly and printing techniques [31, 32]. Screen-printing of capacitive materials onto flexible substrates has been studied for applications in traditional thin film SCs [33, 34]. However, to power some of the future generation wearable devices and smart clothes, it is required to improve the flexibility of the SCs devices beyond that of the traditional polymer substrates. Textiles can provide more flexible substrates, but the devices fabricated so far on textiles suffer from performance stability or the toxicity of the active materials [4, 35, 36].

The problems associated with developing electronic devices on textile are usually related to the highly flexible substrate, which leads to discontinuity of the device components and inconsistency in sending/receiving electric signals. Even with the modern development in nanomaterials and nanomanufacturing techniques, including printing, it is still a challenge to produce electronic devices directly on textile. SC devices that are able to store energy on textile substrates are not an exemption and it was always difficult to obtain reasonable capacity and energy density using any known electrode materials, in addition to maintaining reasonable durability for the device. It has been recently suggested that graphene could be used to make 1D conductive fibres and yarn that could be used as a SC device [36–39]. The fibre was made conductive using both reduced graphene oxide (rGO) ink and another conductive material (Ni particles or CNTs) [36–39]. The conductive fabric was made either by filling a cylindrical tube of Teflon with the active carbonaceous materials or by coating polyester (or cotton) yarns with two layers of Ni current collector and rGO active material. However, there are always some technical problems associated with fabricating wearable textile from these yarn/fibre materials, including the possibility of peeling off the coating during weaving and the slight stiffness of the carbon fibres or metal-coated fibres. Also, it is very difficult to produce large amounts of these fibres and coated yarns with reproducible properties at a reasonable cost.

In the present work, we used a screen-printing method to pattern graphene onto woven cotton textiles. As a consequence of the strong interaction between the hydroxyl groups on the GO and cotton fibres, excellent mechanical stability and flexibility is achieved. We then used a gentle electrochemical reduction method to convert the electrically insulating GO film into a conductive material that served as both the active material and current collector for the SC electrode. The structure of the textile, with its hierarchical porosity in the fibre, yarn and woven or knitted structure, remarkably improved the ion mobility. This is because the graphene electrodes follow the woven and knitted fabric pattern and maintained almost the same free space between individual fibres (2–4 μm) and between yarns (10–30 μm). The present work also showed that the electrode design and aerial mass loading defined the resulting electrochemical performance of the textile SCs. To the best of our knowledge, this is the first report of SC device printed on cotton substrate and a significant step toward realizing 'wearable' electronic devices.

Materials and methods

Electrodes preparation and GO reduction

GO was synthesised from natural graphite by a modified Hummers method, as described elsewhere [40]. A suspension of GO in water with a concentration of 5 mg ml^{-1} was used to print the SC device, the viscosity of which was modified using a acrylate thickening agent in order to achieve desired viscosity (>1 Pa.s) for screen printing paste. This mixture was stirred for 15 min using a overhead mechanical stirrer to produce thick viscous printing paste. The fabric was printed using a hand screen of 62/cm mesh and 10 mm squeegee diameter. A home-made 5-interdigital finger mask were used to print two types of in-plane devices; (I) A millimeter-electrodes device (~2.5 fingers cm^{-1}) with interspaces of 700 μm and (ii) a micro- electrodes device with about ~12 of 700 μm fingers cm^{-1} and

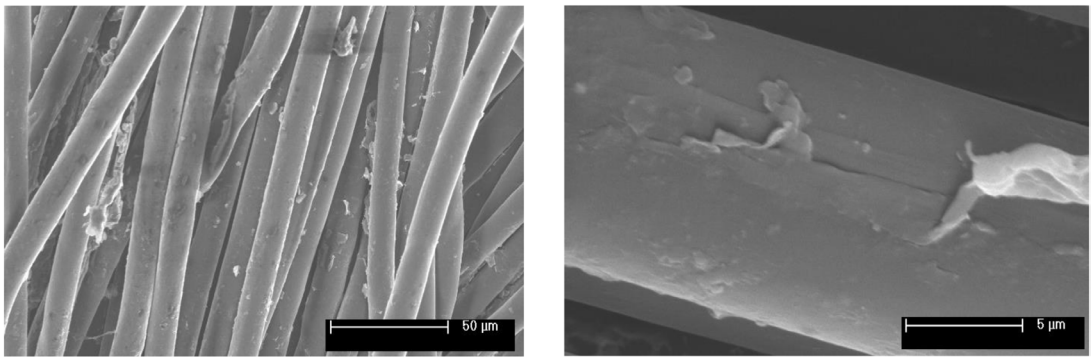

Figure 1. SEM images of rGO coated cotton textile at different magnifications showing uniformity of the coverage. The yarn is well wrapped by graphene so that graphene is very difficult to be distinguished except on the coating defects (right image).

interspaces of 700 μm. All the samples were dried at 100 °C for 5 min using a Werner Mathis laboratory dryer. After printing, the GO was reduced to rGO using an electrochemical method in which the two electrodes of the device were short-circuited using aluminium foil and connected to the negative terminal of a programmable DC power supply (PSS-210-GW INSTEK programmable power supply equipped with Instek PSU software). A steel sheet (10 × 50 × 1 mm) was used as the anode and the electrochemical cell was completed using a 1 M aqueous solution of $FeCl_3$. A potential difference of 2 V was applied across the cell for 60 min and the sample was left in the electrolyte for 120 min after terminating the current. The sample was thoroughly washed with water and dried overnight at 70 °C under vacuum. The total mass of the active materials was ranging between 5–12 mg cm^{-2} (depending on the number of fingers) for each cycle of the screen-printing.

Supercapacitor device fabrication and electrochemical characterisation

The printed rGO electrodes also serve as the current collector. However, copper sheets were glued to the end of every electrode to ensure good electrical contact with the measuring workstation. The printed electrodes were coated with a hydrogel-polymer electrolyte, poly(vinyl alcohol) (PVA) doped with H_2SO_4. The H_2SO_4 PVA gel electrolyte was prepared as follows: 1 g of H_2SO_4 was added into 10 ml of deionized water, and then 1 g of PVA (molecular weight: 89 000–98 000, Sigma-Aldrich) was added. The whole mixture was then heated to 85 °C under stirring until the solution became clear. The electrolyte was drop-casted and left to dry overnight under ambient conditions to ensure that the electrolyte completely wetted the electrode and to allow for evaporation of any excess water. In order to assemble the solid-state sandwiched device, the prepared H_2SO_4 PVA aqueous solution was drop-casted on two graphene-cotton electrodes and dried overnight in air at room temperature to evaporate excess water. Then the two electrodes were pressed together under a pressure of ~1 MPa for 10 min, which allowed the polymer gel electrolyte on each electrode to combine into one thin separating layer to form an integrated device. The electrochemical performances of the printed devices were investigated by cyclic voltammetry (CV), and galvanostatic charge/discharge tests. The electrochemical measurements were performed on an Iviumstat Electrochemical Interface. The CV and galvanostatic charge–discharge measures were conducted in the potential range of −0.2 to 0.8 V at different scan rates and current densities. For measuring the CV at different bending angle, the device was attached to a flexible polyethylene terephthalate film.

Materials characterisation

X-ray photoelectron spectroscopy (XPS) was completed using a Kratos Axis Ultra x-ray photoelectron spectrometer equipped with an aluminium/magnesium dual anode and a monochromated aluminium x-ray source. Fourier-transform infrared (FTIR) spectroscopy was performed at room temperature using a Varian 3100 FTIR spectrometer. The samples were grounded with potassium bromide and then pressed into disks. Thermogravimetric analysis (TGA) was performed using a Jupiter Netzsch STA 449 °C instrument heated at 10 °C min^{-1} from room temperature to 700 °C under a nitrogen gas flow. X-ray diffraction (XRD) analysis was conducted using a Philips X'PERT APD powder x-ray diffractometer ($\lambda = 1.54$ Å, CuKα radiation). Raman spectra were obtained using a Renishaw 1000 spectrometer coupled to a 633 nm He–Ne laser. The laser spot size was ~1–2 μm and the power was approximately 1 mW when the laser was focused on the sample using an Olympus BH-1 microscope. Scanning electron microscopy (SEM) was performed using a Philips XL30 FEG SEM, operating at an accelerating voltage of 5 kV.

Results and discussion

In this work, we used a screen-printing technique to print GO patterns on woven cotton fabric. We found that the GO flakes are uniformly coated on the individual yarns, even after reduction (figure 1). Bending, stretching and even subjecting to a stream of water were found

to have almost no damaging effect on the structural integrity of the coating, even at the microscopic level (figure S8 in the supporting information (stacks.iop.org/TDM/4/035016/mmedia)). The flexibility of the textile was further confirmed by squeezing and pulling a tied textile to form an overhand knot. Furthermore, the mechanical adhesion tests for GO to cotton textile by the standard tape test show no visible GO flake delamination on the tape. The strong lateral cohesion of the adjacent GO sheets in membranes, fibres and coatings was reported in the literature and is attributed to two reasons: (1) the strong van der Waals interactions (from the hydrophobic polyaromatic nano-graphene domains remaining on the basal planes) and (2) the formation of hydrogen bonds through the oxygen functional groups and water molecules on the surface of the GO flakes [41, 42]. The strong adhesion between the GO coating and cotton fibres can be attributed to the same reason, together with the large water absorption of the hydrated GO flakes on cotton fibres [4]. The superior adhesion of GO on cotton fibre is crucial for SC device stability.

Despite the clear mechanical stability of the printed GO on textile, GO is an electrical insulator since most of the carbon atoms in this material are sp^3-hybridised [43, 44]. The electric conductivity increases by increasing the carbon to oxygen ratio (C/O ratio is typically between 1.8 to 2.3 for GO) [18, 44], which can be achieved via several chemical and thermal reduction processes [45]. The strong chemical or thermal reduction methods can produce rGO with conductivity as high as several thousands of S/m [45]. However, most of these processes require high temperatures or harsh chemical environments, which may have a detrimental effect on the textile substrate. In addition, the chemical reduction sometimes uses toxic agents, such as hydrazine, which limits the application of the printed materials in wearable devices. Therefore, we developed an effective *in situ* reduction method that uses a mild electrochemical reaction to remove the oxygen functional groups from the surface of the GO and restore the properties of the pristine graphene. Figure 2 shows the procedure used to fabricate the in-plane SC. Typically, the two electrodes were electrically connected together using thin aluminium foil and attached on glass slide to the negative terminal of a DC power supply. The anode of the cell was a steel slide and the electrolyte was 1 M of $FeCl_3$. After 60 min of applying 2 V across the cell, the anode was removed and the textile piece with the printed electrodes was kept in the electrolyte for another 120 min. The sample was then thoroughly washed with water. The reduction was clear from changing the colour of the printed electrode from brown to black. The mechanical adhesion between the rGO and cotton textile was again tested after reduction by the standard tape test and washing in water, and showed no visible graphene flakes in the solution or on the tape. The adhesion was strong enough that it required 120 min of strong sonication in a water bath to delaminate some of the rGO flakes, which were then subjected to systematic characterisation in order to understand the chemical composition of the GO after reduction.

The chemical composition of rGO was first determined by XPS. The C1s spectra of GO before and after electrochemical reduction are shown in figures 3(a) and (b). For the original GO, the spectrum shows two main peaks that can be fitted to four components arising from C–O groups (hydroxyl and epoxy, ~286.5 eV), the C–C bond (~284.6 eV), C=O (carbonyl, ~288.3 eV) groups and O–C=O (carboxyl, ~290.3 eV) groups [46, 47]. After reduction, the peaks associated with the oxygen functional groups significantly diminished and the spectrum in general exhibits a similar shape to natural graphite (figure S3). The small peak around 288.5 eV indicated some residual oxygen functionality and it is within the ketone and carboxyl carbon region. The C/O ratio of the electrochemically rGO is 8, which is comparable with other reduction methods in the literature (table S1 in the supporting information).

Figure 3(c) shows the representative Raman spectra of GO and rGO. The Raman analysis points were chosen randomly on both fingers of the pattern. Both samples showed D and G peaks at ca. 1349 and 1594 cm^{-1}. The G peak corresponds to the E_{2g} mode observed for sp^2 carbon domains. The D peak is associated with the vibrations of carbon atoms with sp^3 electronic configuration of disordered graphene [48, 49]. The intensity ratio of the D and G bands, I_D /I_G, decreased from 1.2 to 0.9. Such a decrease in the intensity ratio is attributed to the decrease of the sp^3 domains. The thermal gravimetric analysis also confirmed the removal of oxygen containing functional groups. The TGA curve of GO (figure S3, supporting information) shows two peaks for mass loss with increasing temperature: (1) approximately 8% mass loss before 100 °C, which can be attributed to the removal of absorbed water, and (2) approximately 30% at around 200 °C, which can be ascribed to the decomposition of labile oxygen functional groups to form O_2, CO, CO_2 and H_2O gases. The rGO exhibits much higher thermal stability in comparison with GO due to the deoxygenation of GO. The TGA curve of rGO show no peaks during the heating process and a mass loss of only 9 wt.% was found up to 800 °C, which is probably due to some small amount of oxygen containing functionalities, indicating effective removal of the labile oxygen functional groups through the electrochemical reduction.

Furthermore, the FTIR results agreed with other analytical techniques. Figure 3(d) shows the FTIR spectra of GO and rGO. The presence of intrinsic oxygen functionalities on GO is clearly revealed by several vibrational peaks. The vibrational peak at 3430 cm^{-1} is attributed to the −OH group, the peaks at 1718 and 1575 cm^{-1} correspond to the C=O and C–O of the carboxyl moiety, while the peaks at 1210 and 1045 cm^{-1} are ascribed to the C–O stretching of

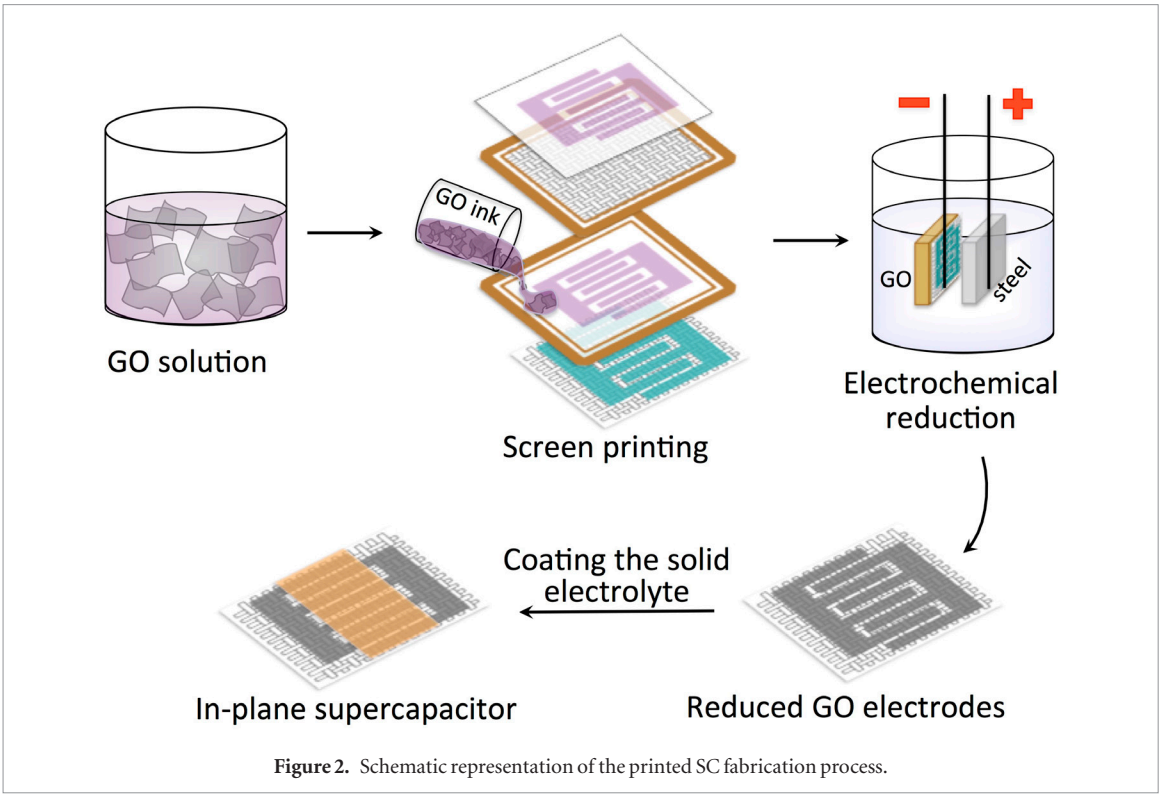

Figure 2. Schematic representation of the printed SC fabrication process.

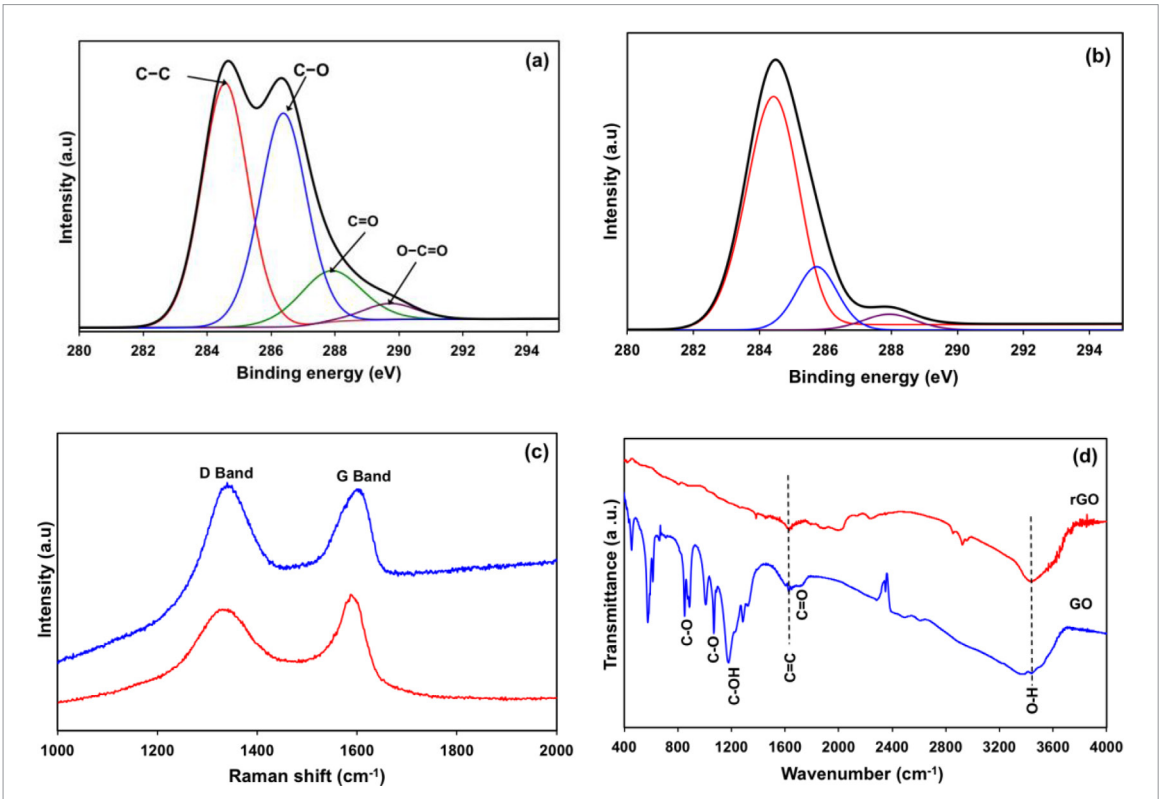

Figure 3. XPS (a) and (b), Raman (c) and FT-IR (d) of GO and rGO showing the efficiency of the electrochemical reduction.

the C–OH and C–O–C moieties, respectively [18, 45]. After the electrochemical reduction, the peaks for oxygen functional groups almost vanished, confirming their efficient removal. The peak at 1625 cm^{-1} corresponding to the aromatic C=C group was still present, suggesting that the frame of sp^2-bonded carbon atoms was retained well after reduction. The Raman results also suggest that the electrochemical reduction is not altering or damaging the flakes (in agreement with Raman).

To complete the SC device, the printed electrodes were coated with a hydrogel-polymer electrolyte, poly (vinyl alcohol) (PVA) doped with H_2SO_4. A sandwich-type SC was also tested for comparison (supplementary information). The CV was first used to evaluate the electrochemical performance of the device. We carried out

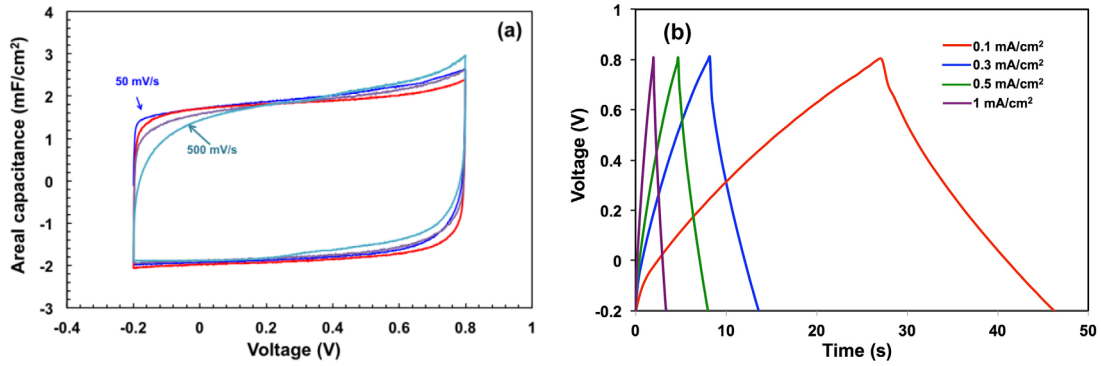

Figure 4. Electrochemical characterisation of the printed graphene on textile. (a) CV at different scan rates and (b) charge/discharge curves at different current densities.

CV measurements in a region between −0.2 to 0.8 V to avoid any irreversible reaction from the electrolyte. The cyclic voltammograms (figure 4(a)) are near rectangular in shape, confirming the formation of an efficient electrochemical double-layer capacitor. The absence of any obvious redox peaks was an indication of the efficient removal of the oxygen functional groups during reduction and therefore the contribution of pseudocapacitance was negligible. With increasing scan rate, CV curves presented good mirror images with respect to the zero-current line and a symmetric *I–E* response at both positive and negative polarisations, implying fast charge transfer within the printed electrode as a result of the highly porous morphology. Even at a scan rate as high as 500 mV s^{-1}, the CV curves remained nearly rectangular without obvious distortion. Galvanostatic charge/discharge curves were also recorded for practical capacitance evaluation. The SC device retained nearly symmetric charge/discharge profiles even at high current density (figure 4(b)). These observations are consistent with the results from CV measurements, further indicating the excellent capacitive behaviour of EDLC. Moreover, the voltage drop at the beginning of each discharge curve, known as the *iR* drop, was small. This is an indication of a low overall internal resistance of the electrode due to the removal of the oxygen functional groups. It is worth mentioning here that the capacitance that a given electrode is able to supply is usually expressed as volumetric capacitance or gravimetric capacitance. However, in our case, the areal capacitance is the most relevant and more practical measure of the capacitance, considering that in a flexible SC, multiple device components are printed onto a given area of the textile substrate. We have tested the influence of the areal loading by repeating the screen-printing for a number of cycles. Figure S6(b) (supporting information) shows the calculated aerial capacitance as a function of the number of the repeated screen-printing cycles measured at a scan rate of 100 mV s^{-1}. Although the mass loading of the active material per unit area increased by three orders, the change in the aerial capacitance is minor. This can be explained by the strong interaction between the GO layers, which reduces the permeability of the coating, making the change in the accessible surface area minor, even with higher loading of the active material.

Interestingly, we found that upon decreasing the discharge time below 1.2 s, noticeable deviations from the ideal capacitance occur. This can be concluded by observing the CV at scan rates above 800 mV s^{-1}. Although this kind of behaviour is conventionally attributed to the limited ionic diffusion of the solid-state electrolyte to the electrodes, we observed that the electrode resistance contributes more to the ideal capacitance deviations than the diffusion. In an ideal scenario, where the capacitance is not limited by the electrolyte accessibility or the electrode conductivity, the aerial capacitance is the slope of the line described by the equation $i = C_I\nu$ where C_I is the ideal areal capacitance, ν is the scan rate and I is the current density. Therefore, plotting the current density versus the scan rate should lead to a linear relation, as in the case that was almost maintained below 800 mV s^{-1}. In the case where there are ionic or electronic limitations, the areal capacitance is less than the ideal case and the current density can be described by equation (1):

$$i = C_I\nu - C_I\nu e^{-t/RC} \quad (1)$$

where R is the resistivity of the cell and C is the measured capacitance. The factor RC is usually referred to as the time constant τ. It is clear from equation (1) that the cell is approaching the ideal behaviour at low scan rates or when the value of τ is much smaller compared to the discharge time. Figure 5(a) plots the value of i as a function of the scan rate ν at 0.3 V. It is clear that the near ideal capacitive behaviour dominates over a wide range of scan rates and only above ~800 mV s^{-1} is a noticeable deviation observed. Figure 5(a) shows also that the onset of the deviation is shifted toward higher scan rate values for the samples with higher aerial loading (more printing cycles). Taking into account that the resistivity of the electrode dropped by four folds when the number of the coated layers increased from three to ten layers (410–110 KΩ sq^{-1}), one can correlate the transport limitation to the resistivity of the electrode. The other factors that may contribute to the shift of the deviation onset, such as electrolyte resistivity and ionic diffusion, are independent of

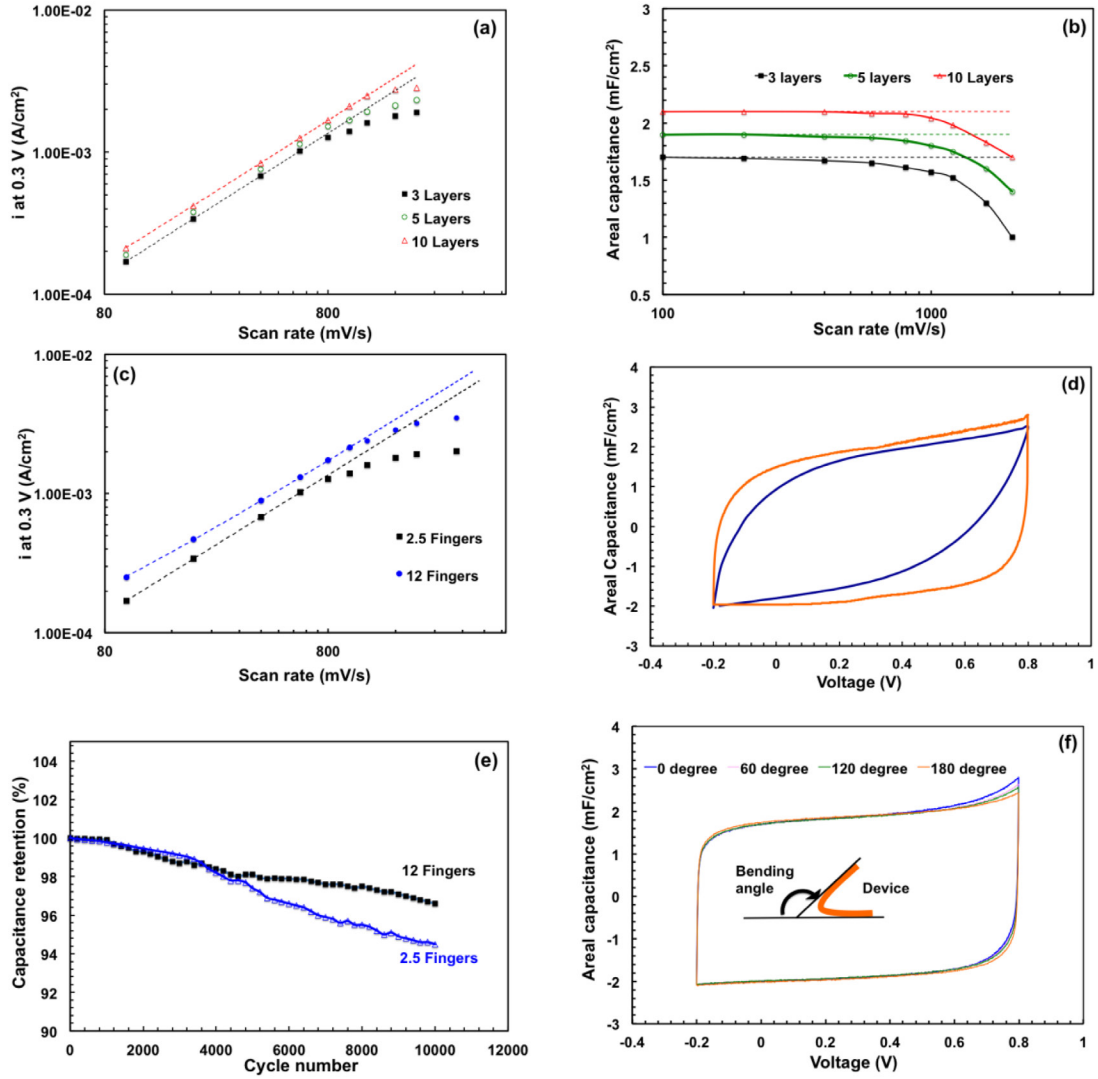

Figure 5. Performance of the printed graphene SC on textile. (a) Current density calculated from the CVs at 0.3 V for different numbers of coating cycles measured at various scan rates. Dashed lines are the intercepts of the ideal capacitance behaviour and allow for extraction of the rate-independent areal capacitance. (b) Value of the areal capacitance plotted as a function of the scan rate after different printing cycles. The dashed lines are the extrapolation of the value of the capacitance at low scan rate, which indicate the deviation from ideal behaviour at the rate-dependent region. (c) Current density obtained from the CV curves at 0.3 V as a function of the current density for different numbers of electrode fingers per unit area. (d) CV curves measured at 1400 mV s^{-1} for the device with different numbers of electrode fingers per unit area. Printed microelectrodes (in orange, 12 electrode fingers per unit area) are clearly more stable at high scan rates. (e) Cyclic stability of the device with different electrodes fingers per unit area measured using the galvanostatic charge/discharge method at 1 mA cm^{-2}. (f) CV curves of the flexible solid-state device at 100 mV s^{-1} for different bending angles.

the number of coating layers and therefore their contribution is minimal.

It is not only the onset of the deviation shift that is noticeable for the more resistive electrodes, but also the value of this deviation at the same scan rate. Practically the measured areal capacitance (C) at certain scan rates in the conditions where there are electronic or ionic limitations is given by the total charge (q) passed divided by the voltage window (ΔV) and the total area (A), according to equation (2) [50]. This value can be calculated form the CV curve by integrating the CV data according to equation (3) [50]. Figure 5(b) plots the value of measured areal capacitance as a function of the scan rate for samples with different loadings. The ideal areal capacitance (C_I) was also plotted by extrapolation of the capacitance value at low scan rates. The value of the C_I–C is larger for the sample with less graphene. This means we may need to increase the number of printed cycles, i.e. the loading of graphene, for the large devices in order to maintain good capacitance.

$$C = \frac{\Delta q/\Delta V}{A} \tag{2}$$

$$C = \frac{\int_V^{V+\Delta V} \mathrm{i}\Delta V}{A \cdot \Delta V \cdot \nu}. \tag{3}$$

The configuration and the design of the electrode also play an important role in the extracted power and energy of the SCs. For the same number of coating layers and the same ratio of covered and uncovered areas,

the value of τ decreased with increasing number of electrode fingers per unit area, as seen from figure 5(C). The deviation from ideal capacitance also shifted toward higher scan rates. This can be explained by reducing the ionic diffusion pathway between the two electrodes. Coupled with the unique porous structures of the printed electrodes, the microelectrode configuration maximises the electrolyte/electrode interface, resulting in the increased capacitance and fast charge/discharge rates. In agreement with this conclusion, the charge/discharge galvanostatic test showed an increase of the areal capacitance from 1.7 to 2.5 mF cm^{-2} (corresponding to about 257 F g^{-1}) when the number of electrode fingers increased from 2.5 to 12 per cm. Also, the charge/discharge curve showed a decrease of the IR drop by increasing the number of electrodes fingers per unit area. The decrease in the IR drop is also an indication of an increase in the power density to reach to a maximum value for the microelectrodes. The obtained value of capacitance in the current work is comparable with the reported value of carbon nanotube coated fabric fixable electrode and even higher than the value reported for rGO rigid electrodes (table S2 in the supporting information) [4, 27].

The electrical cycle lives of the printed graphene flexible SC were also characterised by the galvanostatic charge/discharge method. Figure 5(e) shows the relation between the calculated capacitance and the number of cycles. Although all electrodes exhibited excellent cyclic stability, the microelectrode device was more stable and retained 96.5% of its initial specific capacitance after 10 000 cycles. These results indicate that the printed SC devices exhibit excellent rate capability and a high degree of reversibility at high charging/discharging rates. For practical reasons, it is better to test the device for wearable applications. We recorded the CV of the device at different angles ranging from 0° (unbent) to 180° (folded). Figure 5(f) shows the CV measurements at a scan rate of 100 mV s^{-1} at different bending angles. The CV curves showed little change up to a bend angle of 180°, reflecting that the printed graphene electrodes soaked with polymer gel electrolyte are flexible. We also measured the real capacitance after applying 120% strain for 100 times and no change in the specific capacitance was observed. We then measured the stability of the device at simulated wearing conditions by folding the device to 180° for 2000 cycles. The device maintained 95.6% of the original measured capacitance, indicating the high mechanical integrity and stability even when tested under extreme bending conditions. Furthermore, we have tested the device after washing in a stream of water, and the measured capacitance was almost the same. Such excellent device durability can be attributed to the high mechanical flexibility of the printed graphene electrodes on cotton textile coupling with elastic polymer gel electrolyte. The electrolyte solidifies during the device assembly and acts as a flexible coating that prevents the peeling off the graphene electrodes and also act as glue that holds the graphene flakes on the electrodes together, reducing the chance of cracking the electrode [51].

Conclusions

A flexible and durable SC device was fabricated by printing GO on cotton textile. The printed electrodes were first reduced using electrochemical techniques in aqueous solution. The reduction methods were able to remove most of the oxygen functional groups from the surface of the graphene exposed to the electrolyte, providing a conductive interconnected network. The conductive network performed both as a current collector and an active SC material. The obtained aerial capacitance was as high as 2.5 mF cm^{-2} and maintained 95.6% of these values when tested under bending conditions. The solid-state SC device exhibited superior electrochemical stability and maintained 97% of its original capacitance after 10 000 cycles, which is to our knowledge, the most stable device fabricated on textile.

Acknowledgments

This work was supported by the EU Graphene Flagship Program, European Research Council Synergy Grant Hetero2D, the Royal Society, Engineering and Physical Research Council (UK), US Army Research Office. Authors also acknowledge the support of the Centre for Innovative Manufacture of Large Area Electronics and the National Graphene Institute. Authors kindly acknowledge EPSRC Impact Acceleration Account IAA Grant 110: Knowledge Exchange Fellow (Graphene) for Dr Nazmul Karim; The Government of Bangladesh for PhD Scholarship of Shaila Afroj.

ORCID

Amr M Abdelkader https://orcid.org/0000-0002-8103-2420
Nazmul Karim https://orcid.org/0000-0002-4426-8995
Cristina Valles https://orcid.org/0000-0002-9359-1705
Shaila Afroj https://orcid.org/0000-0002-0469-261X
Kostya S Novoselov https://orcid.org/0000-0003-4972-5371
Stephen G Yeates https://orcid.org/0000-0003-1190-2280

References

[1] Kim D H and Rogers J A 2008 Stretchable electronics: materials strategies and devices *Adv. Mater.* **20** 4887–92

[2] Anliker U et al 2004 AMON: a wearable multiparameter medical monitoring and alert system IEEE Trans. Inf. Technol. Biomed. 8 415–27
[3] Gwon H et al 2011 Flexible energy storage devices based on graphene paper Energy Environ. Sci. 4 1277–83
[4] Hu L et al 2010 Stretchable, porous, and conductive energy textiles Nano Lett. 10 708–14
[5] Meng C, Liu C, Chen L, Hu C and Fan S 2010 Highly flexible and all-solid-state paperlike polymer supercapacitors Nano Lett. 10 4025–31
[6] Meng F and Ding Y 2011 Sub-micrometer-thick all-solid-state supercapacitors with high power and energy densities Adv. Mater. 23 4098–102
[7] Lu X, Yu M, Wang G, Tong Y and Li Y 2014 Flexible solid-state supercapacitors: design, fabrication and applications Energy Environ. Sci. 7 2160–81
[8] Cheng Y, Lu S, Zhang H, Varanasi C V and Liu J 2012 Synergistic effects from graphene and carbon nanotubes enable flexible and robust electrodes for high-performance supercapacitors Nano Lett. 12 4206–11
[9] Wang K, Meng Q, Zhang Y, Wei Z and Miao M 2013 High-performance two-ply yarn supercapacitors based on carbon nanotubes and polyaniline nanowire arrays Adv. Mater. 25 1494–8
[10] Fu Y et al 2012 Fiber supercapacitors utilizing pen ink for flexible/wearable energy storage Adv. Mater. 24 5713–8
[11] Niu Z et al 2011 Compact-designed supercapacitors using free-standing single-walled carbon nanotube films Energy Environ. Sci. 4 1440–6
[12] Pech D et al 2010 Ultrahigh-power micrometre-sized supercapacitors based on onion-like carbon Nat. Nanotechnol. 5 651–4
[13] Deng L et al 2013 Supercapacitance from cellulose and carbon nanotube nanocomposite fibers ACS Appl. Mater. Interfaces 5 9983–90
[14] Sumboja A, Foo C Y, Wang X and Lee P S 2013 Large areal mass, flexible and free-standing reduced graphene oxide/manganese dioxide paper for asymmetric supercapacitor device Adv. Mater. 25 2809–15
[15] Meng Y et al 2013 All-graphene core-sheath microfibers for all-solid-state, stretchable fibriform supercapacitors and wearable electronic textiles Adv. Mater. 25 2326–31
[16] Wu Q, Xu Y, Yao Z, Liu A and Shi G 2010 Supercapacitors based on flexible graphene/polyaniline nanofiber composite films ACS Nano 4 1963–70
[17] Xia J, Chen F, Li J and Tao N 2009 Measurement of the quantum capacitance of graphene Nat. Nanotechnol. 4 505–9
[18] Dikin D A et al 2007 Preparation and characterization of graphene oxide paper Nature 448 457–60
[19] Zhu Y et al 2011 Carbon-based supercapacitors produced by activation of graphene Science 332 1537–41
[20] El-Kady M F, Strong V, Dubin S and Kaner R B 2012 Laser scribing of high-performance and flexible graphene-based electrochemical capacitors Science 335 1326–30
[21] Sun Y, Wu Q and Shi G 2011 Graphene based new energy materials Energy Environ. Sci. 4 1113–32
[22] Zoromba M S, Abdel-Aziz M H, Bassyouni M, Gutub S, Demko D and Abdelkader A 2017 Electrochemical activation of graphene at low temperature: the synthesis of three-dimensional nanoarchitectures for high performance supercapacitors and capacitive deionization ACS Sustain. Chem. Eng. 5 4573–81
[23] Xu Y, Sheng K, Li C and Shi G 2010 Self-assembled graphene hydrogel via a one-step hydrothermal process ACS Nano 4 4324–30
[24] Huang X, Qi X, Boey F and Zhang H 2012 Graphene-based composites Chem. Soc. Rev. 41 666–86
[25] Yu D and Dai L 2010 Self-assembled graphene/carbon nanotube hybrid films for supercapacitors J. Phys. Chem. Lett. 1 467–70
[26] Abdelkader A M, Vallés C, Cooper A J, Kinloch I A and Dryfe R A W 2014 Alkali reduction of graphene oxide in molten halide salts: production of corrugated graphene derivatives for high-performance supercapacitors ACS Nano 8 11225–33
[27] Abdelkader A M 2015 Electrochemical synthesis of highly corrugated graphene sheets for high performance supercapacitors J. Mater. Chem. A 3 8519–25
[28] Duffy N W, Baldsing W and Pandolfo A G 2008 The nickel–carbon asymmetric supercapacitor-performance, energy density and electrode mass ratios Electrochim. Acta 54 535–9
[29] Jost K et al 2011 Carbon coated textiles for flexible energy storage Energy Environ. Sci. 4 5060–7
[30] Yang X, Zhu J, Qiu L and Li D 2011 Bioinspired effective prevention of restacking in multilayered graphene films: towards the next generation of high-performance supercapacitors Adv. Mater. 23 2833–8
[31] Chee W K, Lim H N, Zainal Z, Huang N M, Harrison I and Andou Y 2016 Flexible graphene-based supercapacitors: a review J. Phys. Chem. C 120 4153–72
[32] Xu Y, Lin Z, Huang X, Liu Y, Huang Y and Duan X 2013 Flexible solid-state supercapacitors based on three-dimensional graphene hydrogel films ACS Nano 7 4042–9
[33] Wan X, Huang Y and Chen Y 2012 Focusing on energy and optoelectronic applications: a journey for graphene and graphene oxide at large scale Acc. Chem. Res. 45 598–607
[34] Li L et al 2016 High-performance solid-state supercapacitors and microsupercapacitors derived from printable graphene inks Adv. Energy Mater. 6 1600909
[35] Kou L et al 2014 Coaxial wet-spun yarn supercapacitors for high-energy density and safe wearable electronics Nat. Commun. 5 3754
[36] Liu L, Yu Y, Yan C, Li K and Zheng Z 2015 Wearable energy-dense and power-dense supercapacitor yarns enabled by scalable graphene–metallic textile composite electrodes Nat. Commun. 6 7260
[37] Jiang W et al 2016 Space-confined assembly of all-carbon hybrid fibers for capacitive energy storage: realizing a built-to-order concept for micro-supercapacitors Energy Environ. Sci. 9 611–22
[38] Zhai S et al 2015 All-carbon solid-state yarn supercapacitors from activated carbon and carbon fibers for smart textiles Mater. Horiz. 2 598–605
[39] Lee J A et al 2013 Ultrafast charge and discharge biscrolled yarn supercapacitors for textiles and microdevices Nat. Commun. 4 1970
[40] Hummers W S and Offeman R E 1958 Preparation of graphitic oxide J. Am. Chem. Soc. 80 1339
[41] Pushparaj V L et al 20074 Flexible energy storage devices based on nanocomposite paper Proc. Natl Acad. Sci. USA 104 13574–7
[42] Yun S, Jang S D, Yun G Y, Kim J H and Kim J 2009 Paper transistor made with covalently bonded multiwalled carbon nanotube and cellulose Appl. Phys. Lett. 95 104102
[43] Abdelkader A M, Kinloch I A and Dryfe R A W 2014 High-yield electro-oxidative preparation of graphene oxide Chem. Commun. 50 8402–4
[44] He H, Klinowski J, Forster M and Lerf A 1998 A new structural model for graphite oxide Chem. Phys. Lett. 287 53–6
[45] Stankovich S et al 2007 Synthesis of graphene-based nanosheets via chemical reduction of exfoliated graphite oxide Carbon 45 1558–65
[46] Yang D-Q and Sacher E 2005 Carbon 1s x-ray photoemission line shape analysis of highly oriented pyrolytic graphite: the influence of structural damage on peak asymmetry Langmuir 22 860–2
[47] Zhao J, Pei S, Ren W, Gao L and Cheng H M 2010 Efficient preparation of large-area graphene oxide sheets for transparent conductive films ACS Nano 4 5245–52
[48] Ferrari A C and Basko D M 2013 Raman spectroscopy as a versatile tool for studying the properties of graphene Nat. Nanotechnol. 8 235–46
[49] Abdelkader A M, Patten H V, Li Z, Chen Y and Kinloch I A 2015 Electrochemical exfoliation of graphite in quaternary ammonium-based deep eutectic solvents: a route for the mass production of graphane Nanoscale 7 11386–92
[50] Stoller M D and Ruoff R S 2010 Best practice methods for determining an electrode material's performance for ultracapacitors Energy Environ. Sci. 3 1294–301
[51] Ibrahim M M and El-Zawawy W K 2015 Extraction of cellulose nanofibers from cotton linter and their composites Handbook of Polymer Nanocomposites Processing, Performance and Application: Volume C: Polymer Nanocomposites of Cellulose Nanoparticles ed Pandey J K et al (Berlin: Springer) pp 145–64